MÜLLER GLIA CO-REGULATE BARRIER PERMEABILITY WITH ENDOTHELIAL CELLS IN AN VITRO MODEL OF HYPERGLYCEMIA

Juan S. Peña[1], Francois Berthiaume[1], and Maribel Vazquez[1]*

[1] Rutgers, The State University of New Jersey

Department of Biomedical Engineering

599 Taylor Road, Piscataway, NJ 08854 USA

* Author to whom correspondence should be addressed: mv582@soe.rutgers.edu

Funding Sources:

National Science Foundation (CBET 2243644)

New Jersey Health Foundation (PC 140-24)

No commercial relationships to disclose

ABSTRACT

Diabetic retinopathy is a complex, microvascular disease that impacts millions of working adults each year. High blood glucose levels from *Diabetes Mellitus* lead to accumulation of advanced glycation end products (AGEs), which promote inflammation and breakdown of the inner blood retinal barrier (iBRB) to result in vision loss. This study used an in vitro model of hyperglycemia to examine how endothelial cells (ECs) and Müller glia (MG) collectively regulate molecular transport. Changes in cell morphology, expression of junctional proteins and reactive oxygen species (ROS) of ECs and MG were examined when exposed to a hyperglycemic medium containing AGEs. Trans endothelial resistance (TEER) assays were used to measure changes in cell barrier resistance in response to hyperglycemic and inflammatory conditions, with and without an anti-VEGF compound. Both cell types responded to hyperglycemic conditions with significant changes in cell area and morphology, ROS, and expression of junctional proteins ZO-1, Cx-43, and CD40, as well as the receptor for AGEs. Resistivities of individual and dual ECs and MG barriers decreased within the hyperglycemia model but were restored to that of basal, normoglycemic levels when treated with anti-VEGF. This study illustrated significant phenotypic responses to an in vitro model of hyperglycemia, as well as significant changes in the expression of key proteins used for cell-cell communication. Results highlight important, synergistic relationships between ECs and MG and how they contribute to changes in barrier function in combination with conventional treatments.

1. Introduction

Diabetic retinopathy (DR) is a leading cause of blindness among working adults worldwide, projected to affect more than 160 million people by 2045 [1]. Therapies to treat DR in aging adults face significant challenges, as vision is often diminished via concurrent pathologies that include aberrant angiogenesis, wide-spread retinal hemorrhage, and accumulation of pro-inflammatory compounds, such as advanced glycation end-products (AGEs) [2]. The complex progression of DR alters the structure and operation of the inner blood retinal barrier (iBRB), a selective neurovascular tissue that meets the high metabolic demands of vision by regulating molecular transport across circulating blood and retinal tissue [3]. Limited understanding of age-related, pathological changes to neurovascular barriers is a significant challenge to the development of effective therapies for diabetic retinopathy.

The iBRB is primarily composed of endothelial cells, pericytes, Müller glia, and astrocytes, as shown in **Figure 1-A**. Endothelial cells (ECs) line the inner surfaces of retinal capillaries and collaborate with pericytes to help regulate angiogenic responses, cell-to-cell communication, and selective molecular transport [4, 5]. In complement, astrocyte bodies reside in the retinal nerve fiber layer and extend end feet processes to make direct contact with ECs. Müller glia (MG) span the entire thickness of the retina and directly communicate with ECs. Mounting evidence suggests that chronic hyperglycemia of *Diabetes Mellitus* consists of high glucose and accumulation of AGEs that disrupt cell-to-cell communication and iBRB response [6, 7]. In particular, AGEs are well-known to cause overwhelming pericyte death and gliotic scarring that often requires vitrectomy and astrocyte removal [8]. As a result, MG can become significant cell partners to ECs in aging and pathogenic iBRB. As shown in **Figure 1-B**, these cells collectively

support iBRB integrity by stabilizing tight junctions between ECs, e.g., zonula occludens-1 (ZO-1), and heterotypic gap junctions across neuroglia and ECs, e.g., connexin 43 (CX-43), that facilitate ion balance, waste, and glucose transport between cells [9, 10]. How MG and ECs communicate to collectively regulate molecular transport in hyperglycemic conditions prodromal to DR has been understudied and remains incompletely understood.

This project examined the cellular, molecular, and functional changes of Müller glia (MG) and endothelial cell (ECs) barriers in response to prolonged exposure to high glucose and AGEs typical of hyperglycemia. The conditions stimulated an in vitro, chronic inflammatory state, as evidenced by increased levels of reactive oxygen species (ROS) and expression of the receptor for advanced glycation end-products (RAGE) and cluster of differentiation (CD-40). Dual cell barriers comprised of adjacent MG and ECs monolayers exhibited greater resistivity – and thus greater barrier function – than cell barriers of ECs alone. Moreover, the in vitro hyperglycemia model decreased resistivity of individual and dual MG and ECs barriers, while treatment with contemporary anti-VEGF compounds restored the resistivity of dual cell barriers to those of basal levels. These insights highlight the importance of strategies for treatments that focus on collective barrier responses and its impact with and without conventional treatments, such as anti-VEGF.

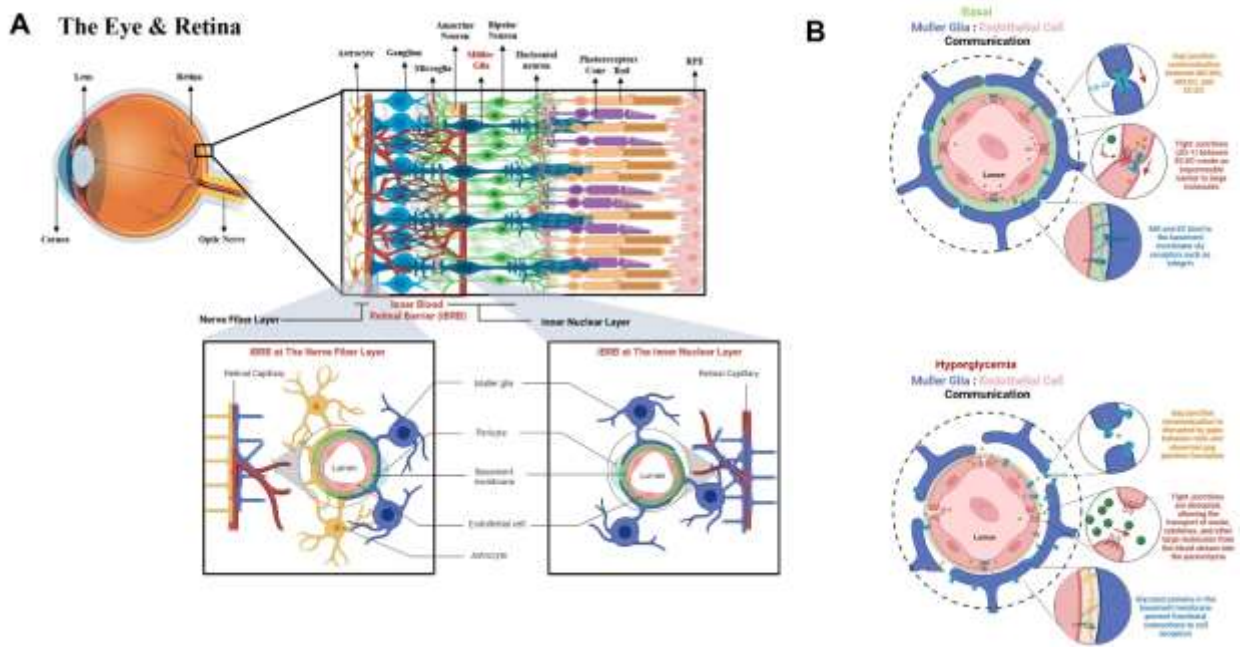

Figure 1. Structure of the inner Blood Retinal Barrier (iBRB) and communication between endothelial cells (ECs) and Müller glia (MG) in basal and hyperglycemic conditions. A) Schematic of the retina and iBRB anatomy. The inner blood retinal barrier is mainly comprised of endothelial cells, pericytes, a basement membrane, and the foot processes of glial cells. The iBRB is a uniform capillary bed extending from the nerve fiber layer to the inner nuclear layer. The foot processes of astrocytes reside on the nerve fiber layer, while the foot processes of Muller glia are throughout the iBRB.

2. Results

2.1. High Glucose and AGEs Induce an In Vitro Hyperglycemic State

Hyperglycemia-conditioned Müller glia (HMG) and Hyperglycemia-conditioned endothelial cells (HECs) demonstrated cellular and molecular differences from MG and ECs when cultured using 3 different hyperglycemic media conditions of M1: 25mM glucose and 1μg/mL AGEs, M2: 25mM glucose and 5μg/mL AGEs, and M3: 25mM glucose and 10μg/mL AGEs. Tests measured expression of reactive oxygen species (ROS), cluster of differentiation 40 (CD40), and the receptor for advanced glycation end-products (RAGE), i.e., known markers upregulated in diabetic rodent retinal cells in vitro, as previously reported [11-13].

2.2. Reactive Oxygen Species (ROS) Expression

HMG and HECs demonstrated significantly higher expression of ROS than MG and ECs in response to hyperglycemic media, as shown in **Figure 2-A**. The upregulated ROS expression in HMG increased by 4.9-fold with respect to MG (6.7% to 32.9%, $p < 0.05$) and in HECs by 3-fold (13.4% to 40.8%, $p < 0.01$) with respect to ECs when exposed to hyperglycemic medium 1, i.e., 25nM glucose and 1μg/mL AGEs. Likewise, ROS expression in hyperglycemic medium 2 (25nM glucose and 5μg/mL AGEs) was upregulated in HMG by 3.2-fold (6.7% to 21.4%, n.s.) and in HECs by 3.5-fold (13.4% to 46.8%, $p < 0.001$). Lastly, ROS expression in hyperglycemic medium 3 (25nM glucose and 10μg/mL AGEs) was upregulated in HMG by 5.7-fold (6.7% to 37.8%, $p < 0.05$) and in HECs by 17.1-fold (13.4% to 57.6%, $p < 0.0001$). Despite that both hyperglycemic medium 1 and medium 3 demonstrated significant upregulation of ROS for both HMG and HECs, hyperglycemic medium 1 yielded cell viability above 90% (data not shown). Hence, hyperglycemic medium 1 was selected for the remainder of this study. **Figure 2-B** shows

representative brightfield and fluorescence images of ROS expression in HMG and HECs on the 6th day post-treatment with hyperglycemic medium 1.

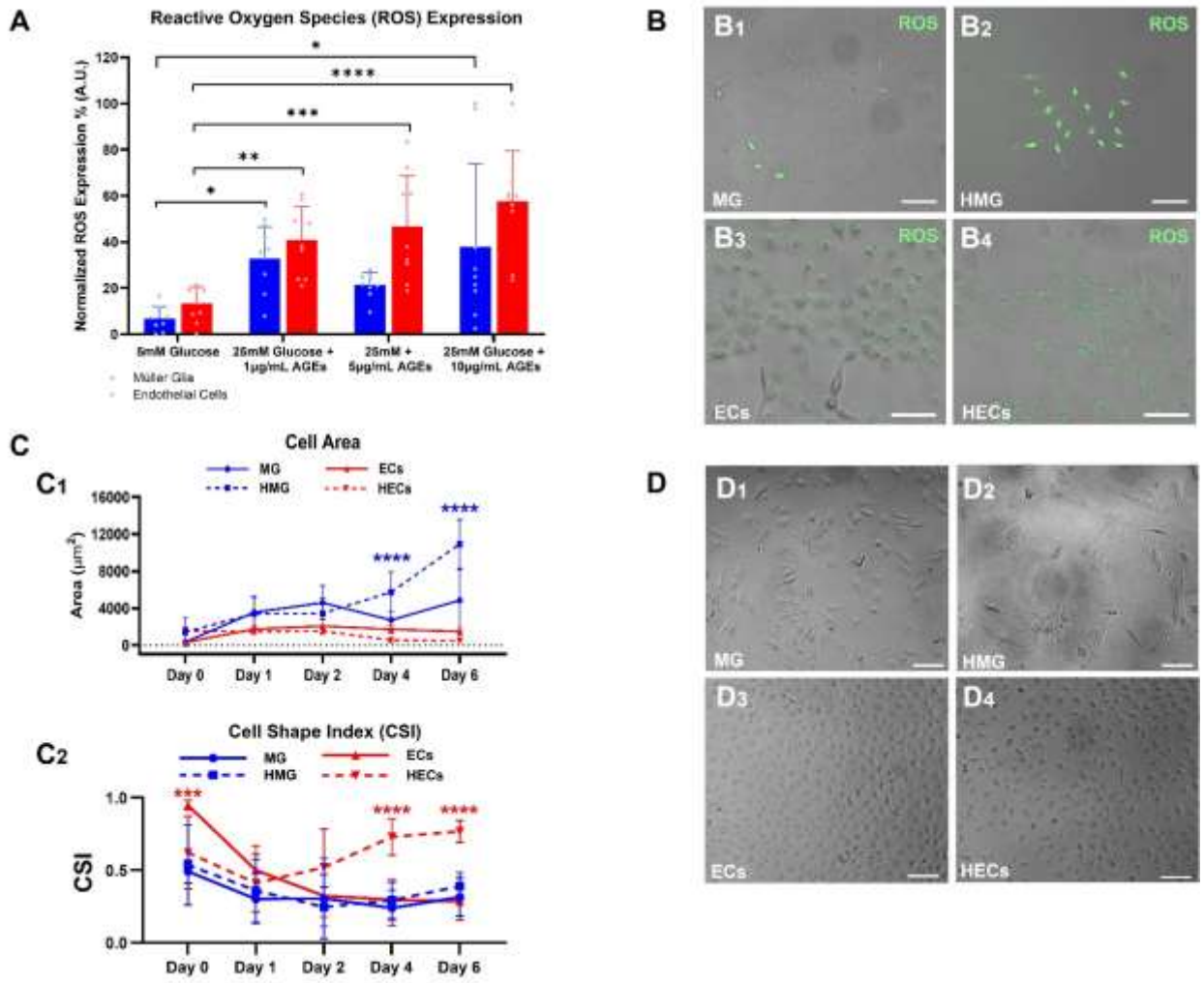

Figure 2. Morphology Changes in Müller Glia (MG) and Endothelial Cells (ECs) in Response to Hyperglycemic Conditions formed using High Glucose and Advanced Glycation End-Products (AGEs). A) Reactive Oxygen Species (ROS) expression in MG and ECs in response to different concentrations of hyperglycemic media: 25mM glucose and either 1µg/mL, 5 µg/mL, or 10 µg/mL of advanced glycation end-products (AGEs) after 6 days of culture. Ultimately the condition of 25mM glucose

142 + 1μg/mL AGEs was chosen as the hyperglycemic media for this study. **B)** Representative brightfield and
143 fluorescence images of ROS expression in **B1)** Müller glia (MG), **B2)** hyperglycemic MG (HMG) – MG
144 exposed to hyperglycemic media, **B3)** endothelial cells (ECs), and **B4)** hyperglycemic ECs (HECs) – ECs
145 exposed to hyperglycemic media, after 6 days in culture with hyperglycemic media. **C1)** Changes in surface
146 area of MG, ECs, HMG, and HECs in response to control media (5mM glucose) and hyperglycemic media
147 (25mM glucose+1μg/mL AGEs). **C2)** Changes in cell morphology over time measured by cell shape index
148 (CSI) of MG, HMG, ECs, and HECs in response to control media (5mM glucose) and hyperglycemic media
149 (25mM glucose+1μg/mL AGEs. **D)** Brightfield images of **D1)** MG, **D2)** HMG, **D3)** ECs, and **D4)** HECs 24
150 hr post-seeding in culture wells. Scale bar is 100μm. *p< 0.05, **p< 0.01.
151
152 **2.3. Hypertrophic Changes in Cell Area**
153 MG cultured in hyperglycemic media 1 (HMG) displayed statistically significant changes in cell
154 area with respect to MG cultured in basal conditions. These changes illustrate increased
155 hypertrophy from Day 0 (D0 =1 hr post-treatment) to Day 6 (D6). The cell area of MG steadily
156 increased over time in basal media with a 14.3-fold increase on Day 6 with respect to Day 0 (D0
157 = 339.1 μm^2, D4 = 4837.9 μm^2, $p < 0.0001$), while the cell area of HMG increased by 7.6-fold (D0
158 = 1431.8 μm^2, D6 = 10937.8 μm^2, $p < 0.0001$) on the 6th day with respect to Day 0. The cell area
159 of MG and HMG was also significantly different on Day 6 (MG = 4837.9 μm^2, HMG = 10937.7
160 μm^2, $p < 0.0001$), as illustrated in **Figure 2-C1**. ECs cultured in hyperglycemic media (HECs) did
161 not display significant changes in cell area with respect to ECs cultured in basal media over time.
162
163 **2.4. Changes in Cell Shape Index (CSI) of hyperglycemic Cells**
164 Phenotypic changes in cell morphology, represented by CSI, decreased over time for the HMG,
165 MG, and ECs groups. By contrast, CSI values of HECs slightly increased, as shown in **Figure 2-**

C2. The average CSI values on day 6 for HMG (CSI = 0.39 ± 0.09), MG (CSI = 0.31 ± 0.13), ECs (CSI = 0.28 ± 0.13), and HECs (CSI = 0.77 ± 0.08), resulted in significant CSI differences between HECs and ECs by a 2.75-fold difference ($p < 0.0001$). Complete cell area values are shown in **Supplemental Figure S-1**.

HMG demonstrated remarkable hypertrophic changes in comparison to MG, as shown in representative images of **Figure 2-D1** and **2-D2**. The hypertrophy of HMG was characterized by longer cellular processes with an average of 76.9 μm ± 26.1 μm in length for HMG and 39.7 μm ± 11.4 μm for MG . **Figure 2-D3** and **2-D4** show the morphology of ECs and HECs, illustrating smaller cell diameters in the HECs group with an average 20.7 μm ± 3.2, while ECs displayed an average diameter of 38.1 μm ± 7.4 μm.

2.5. Hyperglycemia Induces Changes in RAGE and CD40 Expression

Tests measured the expression of RAGE and CD40 in cell groups via immunocytochemistry. Images of **Figure 3-A,B** show the expression of RAGE in all cell groups 24 hr post-cell attachment in well-plates. The expression of RAGE in both HECs and HMG was significantly higher than ECs and MG by 2.1-fold in both groups, as shown in **Figure 3-C**. Note that fluorescence expression in the isotype control (IgG) shows low background intensity to indicate true RAGE expression in all other cell groups. Representative images of **Figure 3-D, E** show expression of CD40 in all cell groups. The puncta expression of CD40 is seen significantly upregulated in the HECs and HMG by 1.7-fold and 3.8-fold with respect to ECs and MG, respectively. Fluorescence expression in the isotype control (IgG) for the CD40 expression reveals low background

expression, significantly lower than the true expression in the hyperglycemic groups. **Figure 3-F** shows significant differences in CD40 expression in ECs, HECs, MG, and HMG.

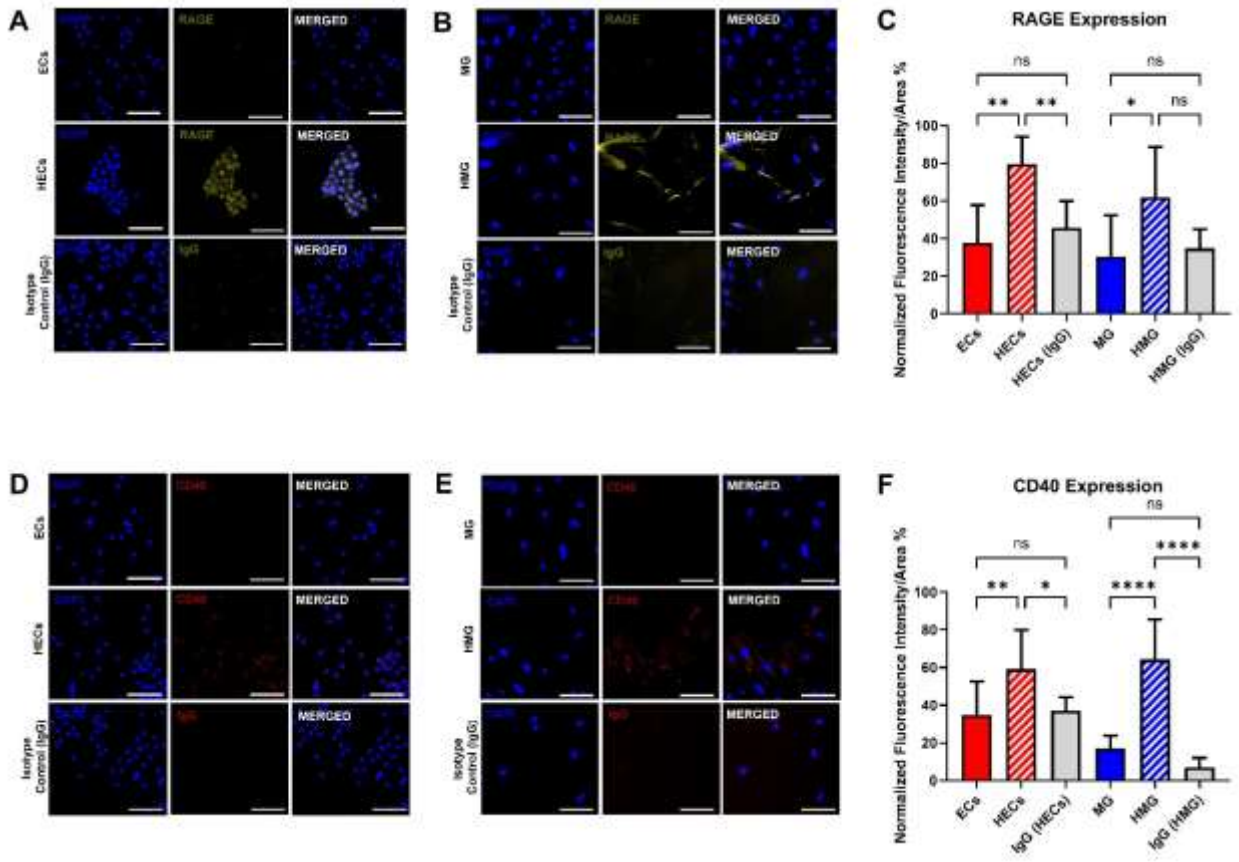

Figure 3. RAGE and CD-40 Expression in ECs, HECs, MG, and HMG. RAGE expression in **A)** endothelial cells (ECs), hyperglycemic endothelial cells (HECs), **B)** Muller glia (MG), and hyperglycemic-induced Muller glia (HMG) cultured in hyperglycemic media (25mM glucose and 1µg/mL AGEs) for 15 days. **C)** Normalized fluorescence intensity per cell area (%) correlating RAGE expression in all cell groups. CD-40 expression in **D)** ECs, HECs, **E)** MG, and HMG cultured in hyperglycemic media (25mM glucose and 1µg/mL AGEs) for 15 days. **F)** Normalized fluorescence intensity per cell area (%) correlating CD-40 expression in all cell groups. IgG was utilized as a negative immunostaining control. Scale bar is 100µm. *p< 0.05, **p< 0.01.

2.6. Zonula Occludens-1 (ZO-1) Expression is Downregulated in HECs

HECs demonstrated a 22.4% decrease in ZO-1 expression ($p < 0.001$) when compared to ECs, as seen in **Figure 4-A**. Localization of ZO-1 in HECs displayed disrupted organization along the cell perimeter, depicting clustering of ZO-1 in different sections of the monolayer (white arrow heads). ZO-1 was mostly found bordering the perimeters of ECs. Likewise, gaps in between HECs were noticeable (yellow arrow heads), caused either by inability to properly link due to disruption in the process of ZO-1 formation, or by degradation of the protein causing gaps in the monolayer.

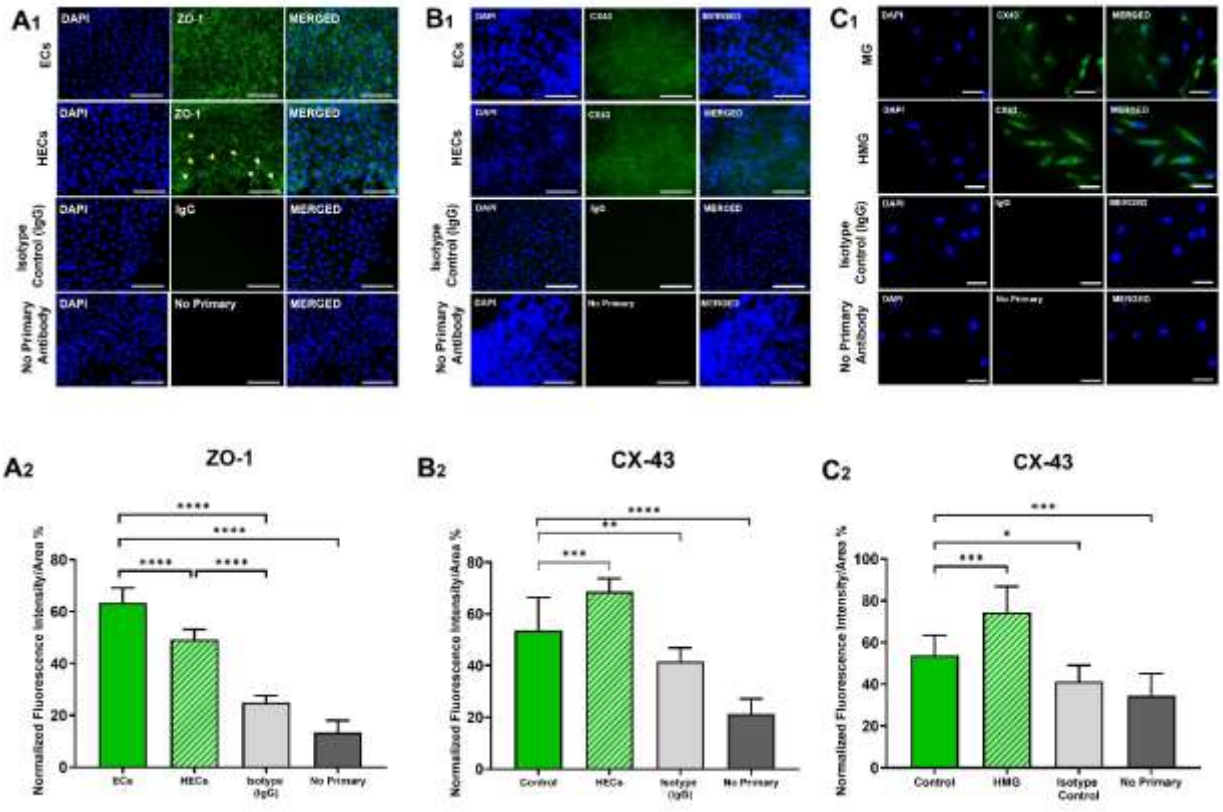

Figure 4. Expression of Zonula Occludens 1 (ZO-1) and Connexin-43 (CX43) Expression in Müller glia (MG) and Endothelial Cells (ECs). A1) ZO-1 expression in ECs in response to hyperglycemic condition (25mM glucose+1µg/mL AGEs), and staining controls (Isotype control and No primary antibody). Yellow arrowheads point towards disruption of ZO-1 boundaries between adjacent cells. White

arrowheads point to clustering of ZO-1. **A2)** Quantification of ZO-1 in ECs via integrated fluorescence intensity/area. **B1)** CX43 expression in ECs in response to hyperglycemic condition (25mM glucose+1μg/mL AGEs), and controls (Isotype control and No primary antibody). **B2)** Quantification of CX43 in ECs via integrated fluorescence intensity/area. **C1)** CX43 expression in MG in response to hyperglycemic condition (25mM glucose+1μg/mL AGEs), and controls (Isotype control and no primary antibody). **C2)** Quantification of CX43 in MG via integrated fluorescence intensity/area. Scale bar is 100μm. * $p< 0.05$, ** $p< 0.01$, *** $p< 0.001$, **** $p< 0.0001$.

2.7. Connexin-43 (CX-43) is Upregulated in HECs and HMG

HECs demonstrated a 28.1% higher expression of CX-43 than ECs ($p < 0.01$), as shown in **Figures 4-B1** and **4-B2**. Expression of CX-43 was observed ubiquitously in the cytoplasm of all cell groups, as per **Figure 4-C1**. The expression of CX-43 in HMG was significantly upregulated by 37.8% ($p < 0.01$) with respect to control as shown in **Figure 4-C2**.

2.8. Barrier Integrity Varies in Hyperglycemic and Basal Conditions

The resistivity of basal (or normoglycemic) and hyperglycemic cell barriers was assessed using TEER measurements over time. Tests first determined the resistance profiles of MG, ECs, and COMBO, as well as HECs, HMG, and hyperglycemic H-COMBO by measuring barrier resistance over the course of 7 days, as per **Figure 5-A**. Differences in cell barrier resistance among basal groups are shown in **Figure 5-B1**, differences among hyperglycemic cell groups are shown in **Figure 5-B2**, and comparisons between normoglycemic cell cohorts and hyperglycemic cohorts are in **Figure 5-B3**.

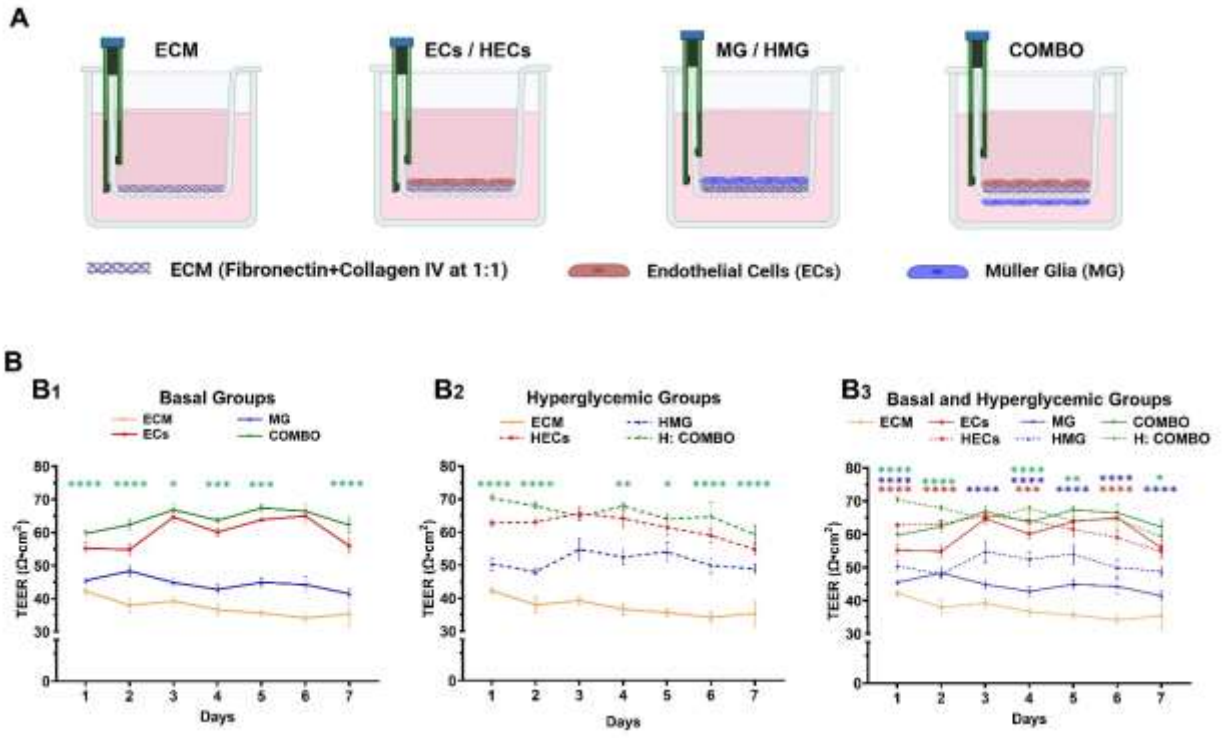

Figure 5. Measurement of Barrier Integrity via Trans-Endothelial/Epithelial Resistance (TEER). A) Schematic depicting the transwell configurations of cell barriers, ECM: transwell membrane coated with fibronectin and collagen IV at a 1:1 ratio, 1mg/mL, ECs: Endothelial cells monolayers on coated membranes with ECM. MG: Müller glia monolayers on coated membranes with ECM. COMBO: ECs monolayer on top of an ECM coated membrane + MG monolayer on the bottom of the same membrane. **B)** TEER quantification of **B1)** normoglycemic and **B2)** hyperglycemic groups, **B3)** overlap of normoglycemic and hyperglycemic cell barriers over the course of 7 days. Statistically significant differences between COMBO and ECs are compared in B1, and between hyperglycemic COMBO and HECs are compared in B2. Statistical differences between normoglycemic and hyperglycemic groups of the same cell type (e.g., MG and HMG) are compared in B3. * ($p<0.05$), ** ($p<0.01$), *** ($p<0.001$), and **** ($p<0.0001$).

As shown in **Figure 5-B1**, ECs (red line) displayed a sharp increase in TEER after day 2 and remained steady until a final decrease on day 7. By contrast, MG (blue line) demonstrated a steady TEER profile over the 7 days with an overall TEER decrease. TEER values of ECs monolayers were consistently higher than those of MG monolayers, and TEER values of COMBO barriers (green line) were higher than both for the full 7 days. Note that significance is denoted by green stars ($p<0.01$ to $p<0.001$) for COMBO conditions against ECs, where TEER values are the closest overall. By contrast, **Figure 5-B2** shows a steady decline in the TEER values of HECs (red dashed line) from day 3 until day 7, while the TEER values of HMG (blue dashed line) varied by less than 10% over time. Further, HMG data exhibited an oscillatory pattern of slightly increasing and decreasing TEER values per day. Despite the sharp TEER decline in HECs, the values remained higher than those of HMG, with a final 12.1% TEER difference between the two groups on day 7. Hyperglycemic H-COMBO (dashed green line) also displayed a steady TEER decline from day 4 until day 7, but the values remained above the TEER data of individual HECs and HMG. On day 7, TEER values of H-COMBO were 8.2% and 21.3% higher than those of individual HECs and HMG barriers, respectively. Significance is denoted by green stars ($p<0.01$ to $p<0.001$) against H-COMBO and HECs, as before. In aggregate, **Figure 5-B3** illustrates the similar TEER patterns between HECs and ECs (red dashed versus red solid lines), where both groups exhibited increases in barrier resistance until day 3, followed by a steady decreased resistance until day 7. TEER values of ECs were slightly higher than the ones of HECs (~2%). By contrast, HMG groups displayed an increased barrier resistance during the first 3 days, followed by an oscillating pattern. Surprisingly, TEER values of HMG groups were greater by 17.8% than the TEER of MG groups on day 7 (blue dashed versus blue solid lines). H-COMBO barriers exhibited a similar oscillatory TEER pattern as HMG, with a downward trend after day 4. Note that green stars denote significance between

276 COMBO and H-COMBO values of TEER, red stars between monolayers of ECs and HECs, and
277 blue stars between MG and HMG monolayers.
278
279 **2.9. Hyperglycemic Cell Barriers React Differently to TNF-α Treatment than basal cell**
280 **barriers**
281 The TEER of EC, MG, and COMBO confluent cell barriers cultured in basal conditions was
282 measured for 6 days, with and without TNF-α treatment, as shown on **Figure 6-A1**. During the
283 first 3 days, the COMBO groups displayed the highest TEER values, followed by the monolayers
284 of ECs, and the MG groups. Upon addition of TNF-α on day 3, the cell barrier resistance of ECs
285 exhibited a 19.3% decrease (inset), MG groups experienced a 10.7% decrease (inset), and the
286 barrier resistance of COMBO groups decreased by 20.9% (inset) over the course of 24 hr.
287 Recovery of cell barrier resistance post removal of TNF-α was measured by calculating the
288 percentage increase in TEER from day 4 to day 6 in all cell barrier groups. As shown in the shaded
289 area of **Figure 6-A1,** MG cell barriers displayed the highest recovery with a 25.2% increase in
290 TEER, followed by ECs with 16.1%, and COMBO groups with 13.5% increase.
291
292 The TEER data of hyperglycemic cell barriers is illustrated in **Figure 6-A2**. The barrier resistance
293 of hyperglycemic barriers was similar to those of basal groups with the highest TEER value
294 measured in the H-COMBO groups, followed by monolayer barriers of HECs, and HMG
295 monolayers. As shown in the inset, addition of TNF-α resulted in a sharp decrease of cell barrier
296 resistance in all hyperglycemic groups. HECs exhibited a 24.5% decrease in TEER, followed by
297 HMG with a 13% decrease, and H-COMBO with a 27% decrease over the 24 hr exposure to TNF-
298 α. In contrast to basal conditions, recovery of hyperglycemic cell barriers post-TNF-α removal was

led by the H-COMBO groups with a 30.1% increase in TEER, followed by a 23% increase in HEC monolayers, and a 15% increase in HMG monolayers, as shown in the shaded area of **Figure 6-A2**.

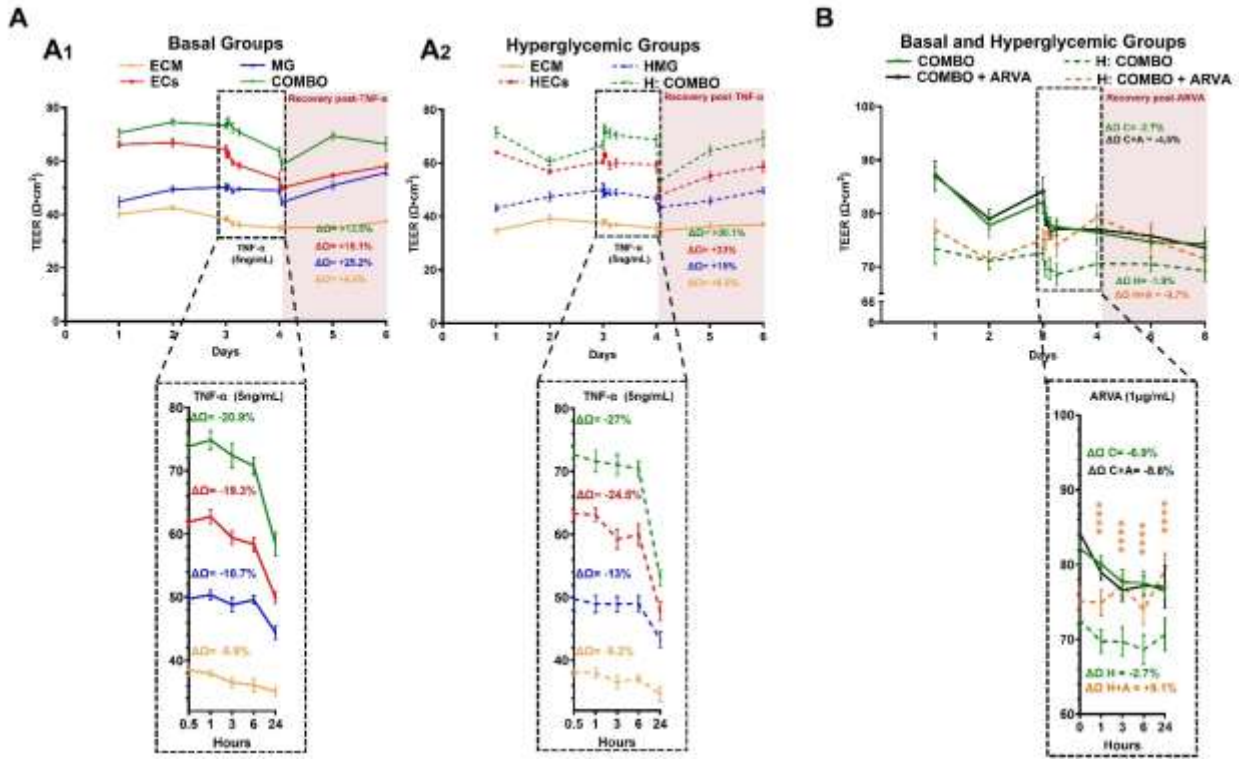

Figure 6. Barrier Recovery Response to TNF-α and ARVA via Trans-Endothelial/Epithelial Resistance (TEER). A) TEER quantification of cell barriers in the presence of TNF-α (5ng/mL) in **A1)** normoglycemic groups (solid lines) and **A2)** hyperglycemic groups (dashed lines). ECM: transwell membrane coated with fibronectin and collagen IV at a 1:1 ratio, 1mg/mL, ECs: Endothelial cells monolayers on coated membranes with ECM. MG: Müller glia monolayers on coated membranes with ECM. COMBO: ECs monolayer on top of an ECM coated membrane + MG monolayer on the bottom of the same membrane. **B)** TEER quantification of cell barriers in the presence of Anti-Rat Vegf-A (ARVA) (1μg/mL) in normoglycemic groups (solid lines) and hyperglycemic groups (dashed lines). COMBO: ECs

monolayer on top of an ECM coated membrane + MG monolayer on the bottom of the same membrane. Hyperglycemic COMBO: COMBO in hyperglycemic conditions. COMBO + ARVA: COMBO treated with ARVA (1μg/mL). Hyperglycemic COMBO + ARVA: hyperglycemic COMBO treated with ARVA (1μg/mL). ΔΩ is the percent TEER recovery, measured by the TEER change between day 4 and day 6. ΔΩ = COMBO, ΔΩ C+A = COMBO +ARVA, ΔΩ D = Hyperglycemic COMBO, and ΔΩ DC + A = Hyperglycemic COMBO +ARVA. **** ($p < 0.0001$) correspond to the statistical difference between hyperglycemic COMBO and hyperglycemic COMBO + ARVA.

2.10. Anti-VEGF Treatment Increased Resistivity of Hyperglycemic Cell Barriers

The final tests exposed COMBO barriers of cells cultured in basal conditions and in hyperglycemic conditions (H-COMBO) to treatment with anti-VEGF (ARVA) and measured changes in barrier resistivity. Note that groups not denoted with ARVA were treated with a simple change in respective media. As seen in **Figure 6B**, basal COMBO groups (solid line) displayed higher TEER values than hyperglycemic H-COMBO groups (dashed lines) in the first 3 days, prior to ARVA treatment. However, the treated basal groups (COMBO + ARVA) displayed a TEER decrease of 8.6% upon exposure to ARVA, while the basal COMBO groups alone exhibited a TEER decrease of 6.9% when treated with a media change (Inset). We note that inset values highlight the larger change in TEER with respect to each barrier. By contrast, treated hyperglycemic groups (H-COMBO + ARVA) experienced a notable and significant 9.1% increase in TEER, while the H-COMBO alone exhibited a slight decrease of 2.7% (Inset). Yellow stars denote significance ($p<0.01$ to $p<0.001$) between TEER values of the treatment groups (COMBO + ARVA) and (H-COMBO + ARVA). As shown, the TEER values of the hyperglycemic groups (H-COMBO + ARVA) after ARVA exceeded those of the basal COMBO group, with and without ARVA. After media was changed to remove ARVA from all targeted groups, TEER values of the (COMBO +

ARVA) group decreased by 4.5% at Day 6, while the TEER of the hyperglycemic (H-COMBO + ARVA) decreased 9.7%, as shown in the shaded area of **Figure 6-B**. Notably, there were no statistically significant differences in TEER values between the basal and H-COMBO conditions with ARVA during the recovery period of Day 4 through Day 6 (ns: $p>0.05$). Lastly, the TEER of COMBO and H-COMBO groups untreated with ARVA decreased by a modest 2.7% and 1.9%, respectively, upon media change (ns with $p>0.05$).

3. Discussion

Diabetic retinopathy is a rising health challenge with a lack of therapies to treat chronic stages in aging adults. Understanding cellular mechanisms that regulate barrier integrity is critical for development of treatments to prevent and/or decelerate vision loss. This study highlights that both Müller glia (MG) and endothelial cells (ECs) respond to an in vitro model of hyperglycemia, with significant changes in cell area and morphology. Further, we observed a synergistic relationship between the two cell types in how they contribute to forming barrier function via changes in protein expression and resistivity.

In vitro models of hyperglycemia using high glucose and advanced glycation end products (AGEs) were able to condition MG and ECs cells into a pro-inflammatory state. While high glucose has been traditionally used to emulate hyperglycemic environments, recent study has suggested that AGEs are an important contributor to the long-term effects of hyperglycemia [14]. Our study examined hyperglycemia by using media with high glucose and 3 different concentrations of AGEs (1μg/mL, 5μg/mL, and 10μg/mL) to illustrate that AGEs upregulated ROS expression and stimulated significant changes in cell area and morphology on both MG and ECs (**Figure 2**). The

selected hyperglycemic condition of 1μg/mL stimulated comparable ROS upregulation in both ECs and MG, which is significant for the study of cooperative transport across dual cell barriers.

Upregulation of the AGEs receptor, RAGE, in both hyperglycemia-induced Müller glia (HMG) and hyperglycemia-induced endothelial cells (HECs) supported a pro-inflammatory state (**Figure 3**). RAGE was localized in HECs nuclei, as reported previously in vitro [15, 16], but largely seen in the cytoplasm of HMG, consistent with vivo studies reporting RAGE localized in the end feet of MG [13, 17]. Moreover, this study is among the first to report expression of CD-40 in HMG using an in vitro model of hyperglycemia (**Figure 3**), as observed in diabetic rats [12, 18] to highlight the significance of in vitro models using AGEs in addition to high glucose.

Next, our data examined dysfunction of tight and gap junction proteins between iBRB cells, which are linked to increased vascular permeability [19, 20]. ZO-1 was significantly downregulated in HECs cultured in our hyperglycemia model (**Figure 4**), consistent with previous in vitro study [9, 21] and with ex vivo study showing increased permeability of retinal microcapillaries from diabetic rodents [22]. We additionally examined Cx-43 expression, as mounting evidence illustrates its crosstalk with the cytoskeleton, focal adhesion complexes, and other junctional structures helps modulate barrier function (reviewed in [23]). Data illustrated significant upregulation of Cx-43 in HECs and in HMG to highlight underexplored influences of Cx-43 on communication between and across these cell groups [10, 24].

The study next examined the influence of our in vitro hyperglycemia model on the resistivity of individual cell barriers formed of ECs and MG groups, alone, as well as in combination barriers

(COMBO), i.e., dual barriers formed by a monolayer of each cell type. Barrier recorded higher TEER values from monolayers of ECs than MG in both normo- and hyperglycemic states (**Figure 5**), consistent with other studies [25] [26] that attributed these differences to downregulation of tight junctions formed across ECs but absent in MG. However, barriers of HMG exhibited surprisingly higher TEER values than normoglycemic MG barriers, which may be attributed to the intrinsic nature of MG that serve as the first line of defense against retinal insults [27]. This increase may also be attributed to MG hypertrophy measured in this study (**Figure 2**), which increases surface area impeding transport and promoting cell-cell communication. Importantly, COMBO barriers exhibited larger TEER values than either cell monolayer, highlighting the significant contribution of MG to transport across this system [11, 28]. Our consistent data are among the first to highlight underexplored roles of MG in co-regulating barrier resistivity with ECs in conditions of hyperglycemia with AGEs.

The last set of experiments examined the changes in resistivity of cell barriers (normo- and hyperglycemic) exposed to inflammatory stimulus via TNF-α and to anti-angiogenic stimulus via ARVA, an anti-VEGF compound. While TEER values of dual cell barriers exposed to TNF-α in COMBO were higher than those of H-COMBO, MG cell barriers displayed the highest TEER recovery once TNF-α stimulus was removed (**Figure 6A**). A surprising 50% increase in MG resistivity was measured over barriers of ECs to suggest a larger contribution of MG to COMBO resistance than previously explored. As seen, the overall increase in barrier resistance of H-COMBO was higher than individual monolayers of HECs or HMG, highlighting a potentially even stronger role of MG to the transport of molecules across hyperglycemic barriers.

406 Experiments lastly evaluated changes in dual barrier resistance to ARVA, a rat anti-VEGF
407 molecule that operates similar to bevacizumab [29, 30]. These tests were significant because they
408 are among the first to examine combinatory influences of anti-angiogenic agents on ECs and MG,
409 with and without hyperglycemia. The TEER of dual barriers cultured in basal conditions
410 (COMBO) was initially higher than that of dual barriers cultured in the hyperglycemia model (H-
411 COMBO), as consistent with the data. However, upon treatment with ARVA, H-COMBO groups
412 exhibited surprisingly robust recovery with TEER values on par with those of normoglycemic
413 conditions ($p>0.05$) (**Figure 6B**). Moreover, COMBO groups displayed decreases in resistivity
414 when first treated with ARVA (inset), while H-COMBO groups treated with ARVA showed
415 increased values of TEER to reach highest levels after ARVA stimulus. This exciting data suggests
416 that anti-VEGF treatments may increase barrier resistance in conditions of hyperglycemia to
417 increase our understanding of the comprehensive impacts of contemporary pharmacology [31].
418
419 **4. Methods and Materials**
420 **4.1. Müller glia (MG) and Hyperglycemia-induced Müller glia (HMG)**
421 Müller glia (MG) cells were isolated from the retina of adult wild-type Sprague-Dawley rats using
422 a Papain dissociation kit (Worthington, NJ). In brief, adult rats were humanely euthanized by CO2
423 asphyxiation following IACUC guidelines. Retinas were extracted and mechanically dissociated
424 into a cell suspension as per protocol [32]. Cells were cultured in Laminin coated flasks with 88%
425 low glucose Dulbecco's Modified Eagle Medium (DMEM) with low glucose (5mM)
426 (ThermoFisher, 12320), 10% Fetal Bovine Serum (FBS) (VWR, 89510-186), and 2%
427 penicillin/streptomycin (VWR, 97062-806) for 9 days. Media was changed every day before
428 lineage characterization. Cells were stained for glial fibrillary acid protein (GFAP), glutamine

synthetase [6], and cellular retinaldehyde binding protein (CRALBP) to identify MG via cell-specific markers, as per established protocols [17, 32].

Hyperglycemia-induced MG (HMG) are defined as MG cultured in DMEM with high glucose 25mM (ThermoFisher, 11965092), 1µg/mL of advanced glycation end products (AGEs) (Sigma Aldrich, 121800-10MG-M), 10% FBS, and 2% penicillin/streptomycin for 15 days before experiments. All cell cultures were kept at 5% CO2 and 37°C.

4.2. Endothelial Cells (ECs) and Hyperglycemia-induced Endothelial Cells (HECs)

Rat primary retinal microvascular endothelial cells (ECs) (Cell Biologics, RA-6065) were cultured in polystyrene flasks with complete endothelial cell medium (Cell Biologics, M1266) containing 2% FBS, 0.1% epidermal growth factor (EGF), 0.1% vascular endothelial growth factor (VEGF), and 1% antibiotic/antimitotic solution.

Hyperglycemia-induced endothelial cells (HECs) are defined as primary rat vein endothelial cells (HECs; Cell Biologics, RD-6009) cultured in polystyrene flasks with complete endothelial cell medium (Cell Biologics, M1266) containing 1µg/mL of advanced glycation end products (AGES) (Sigma Aldrich, 121800-10 MG-M), 2% FBS, 0.1% EGF, 0.1% VEGF, and 1% antibiotic/antimitotic solution. Cultures were kept at 5% CO^2 and 37°C.

4.3. Hyperglycemic Media

Based on previous studies [11, 22], HMG and HECs were exposed to three different hyperglycemic media conditions: (M1) 25mM glucose + 1µg/mL AGEs, (M2) 25mM glucose + 5µg/mL AGEs,

and (M3) 25mM glucose + 10μg/mL AGEs for 6 days, changing the media every other day. Changes in cell morphology were measured each day. After 6 days in culture, the expression of reactive oxygen species (ROS) (ThermoFisher, C6827) and cell viability values from LIVE/DEAD assays (ThermoFisher, R37601) were used to determine the effect of the hyperglycemic media on cells.

4.4. Morphology

Cell morphology was assessed via changes in cell area and cell shape index (CSI), a dimensionless parameter widely used [33, 34] to quantify the roundness of a cell defined in Equation (1).

$$CSI = \frac{4\pi A_S}{P^2} \quad (1)$$

Where A_S is the surface area (μm^2) and P (μm) is the perimeter of the cell. The value of CSI ranges from 0 to 1, where values close to 1 represent a perfectly rounded cell and values approaching 0 denote a fully elongated cell.

This study used a liposaccharide (LPS; MilliporeSigma, L2630) diluted in DMEM at 4μg/mL as a positive control to induce cell area changes in MG and ECs, as per literature [35, 36]. Images of cells in wells were recorded at 1hr, 6 hr, 12 hr, 24 hr, 48 hr, and 72 hr. Cell morphology changes in the hyperglycemia and control groups were performed using the same cell density in well-plates. Note that day zero (D0) values reflect cell morphology 1 hr post-seeding.

4.5. Junction Protein Expression and Localization

Expression and localization of ZO-1 and CX-43 was measured using immunocytochemistry. MG and ECs were seeded in well plates at a concentration $1.0x10^5$ cells/mL in a 24-well plate. After 24 hours, the media was changed to DMEM with low glucose and cells were allowed to grow for 3 days. Media was collected from each culture, filtered (0.2µm pore), and replaced with DMEM. After 24 hr, the media from each culture well was removed and cells were fixed to measure junction protein expression via immunocytochemistry.

4.6. Immunocytochemistry

Briefly, MG, HMG, ECs, and HECs were seeded in 24-well plates (VWR, 29442-044) at a concentration of $1.0\ x10^5$ cells/mL and allowed to attach for 24 hrs. Media from each well was removed, and wells were washed 3 times with Dulbecco's phosphate-buffered saline (DPBS) (Sigma-Aldrich, Cat No. D8537), cells were then fixed with cold paraformaldehyde at 4% for 5 minutes. Wells were washed with DPBS for 5 minutes twice at room temperature. Blocking buffer solution (0.05% Triton X-100, 2% donkey serum, and 3% BSA in DPBS) was added to each well for 15 minutes at room temperature (25C). Following, wells were washed twice with DPBS for 2 minutes, then a primary antibody was added to each well and incubated overnight. The next day, each well was washed 3 times with DPBS for 2 minutes, followed by the addition of the secondary antibody solution for 1 hour at room temperature. Wells were washed with DPBS for 2 minutes 3 times, before adding DAPI (1:1000) into each well for 5 minutes at room temperature. Each well was washed with DPBS 3 times for 2 minutes. Receptor expression was evaluated via fluorescence microscopy (Leica DMi8, NJ).

The primary antibodies used in this study were: CD-40 receptor (ThermoFisher, 500-3704), CRALBP (Life Technologies, PA5100178), CX-43 (ThermoFisher, 71-0700), GFAP (Life Technologies, PA518598)**,** GS Polyclonal Antibody (Life Technologies, 11037-2-AP), Rabbit IgG Isotype Control (ThermoFisher, 02-6102), and RAGE (ThermoFisher, PA1075), ZO-1 (Abcam, ab216880). The secondary antibodies used were: Alexa Fluor™ 488 (ThermoFisher, A-11078), Alexa Fluor 568™ (Life Technologies, A-11057), and Alexa Fluor™ 488 (ThermoFisher, R37118).

4.7. In Vitro Testing System

Transwell assays were used to allow MG and ECs to form individual and dual cell barriers for testing. Transwell inserts with a polyester (PET) membrane (VWR, 29442-082) of 10 μm thickness and 0.4 μm pore size were coated with a solution of Collagen IV (Millipore Sigma, C6745) and fibronectin (Millipore Sigma, F0895) to mimic retinal basement membrane. Briefly, Collagen IV and fibronectin were diluted in DPBS to a concentration of 10μg/mL and mixed in a single solution. Approximately 300 μL of this solution was added to the membrane of each insert and left to crosslink over 24 hours. Following, each insert was washed with DPBS and placed in each well with their respective cell media. MG, HMG, ECs, and HECs were seeded on the top basement membrane-coated membrane individually or in COMBO (i.e., MG with ECs or HMG with HECs). Single cell barriers were seeded at a concentration of $1.0x10^5$cells/mL and left to form confluent monolayers for 48 hr. COMBO conditions required transwell inserts to be flipped upside down and a cell solution of either MG or HMG added on the bottom side of the insert's membrane. Cells were left to attach for 1 hour, then transwells were flipped and placed back in wells containing respective media for 24 hr at 5% CO2 and 37°C. Following, ECs or HECs were added atop

transwell membranes and allowed to attach and form confluent monolayers for 48 hr. Only confluent monolayers validated via brightfield microscopy were used for experiments. Additionally, a transwell insert coated with the basement membrane solution with no cells was used as control (ECM, only).

4.8. Barrier Resistance

The integrity of cell barriers was assessed by measuring the trans-endothelial resistance (TEER) over time. The TEER of confluent cell barriers was measured daily for 7 days using an epithelial voltmeter EVOM2 (Fisher Scientific, NC9792051). The EVOM2's probe (Fisher Scientific, NC9679852) was first calibrated in warm media to reach a baseline TEER value. The baseline number was subtracted from the measured TEER values in each test well.

4.9. TNF-α Treatment

Treatment with tumor necrosis factor alpha (TNF-α) was administered to cell barriers in transwells to measure the ability of cell barriers to restore TEER values of resistance to basal levels. TNF-α was selected because it is an inflammatory cytokine known to reduce cell barrier integrity [37, 38]. Cultures of MG, ECs, HMG, and HECs in well plates were exposed to TNF-α (ThermoFisher,400-14-5UG) diluted in basal media at 1ng/mL, 5ng/mL, or 10ng/mL for 48 hr. TNF-α concentrations were chosen using previous studies that demonstrated the concentrations caused the disruption of barrier integrity in transwell cultures of endothelial cells [38, 39]. A 5ng/mL concentration of TNF-α was chosen for the recovery assays because it demonstrated visible phenotypic changes in cell viability (data not shown).

4.10. Anti-VEGF Treatment (ARVA)

An Anti-VEGF treatment was also administered to cell barriers formed in transwells to measure the impact of VEGF-A inhibition on cell barrier resistance. This study used a rat anti-VEGF-A (ARVA) molecule (Leinco Technologies, V142) that operates in similar fashion as bevacizumab, an anti-VEGF-A agent used to treat aberrant angiogenesis in humans [40]. ARVA at a concentration of 1μg/mL was reconstituted in basal media and administered to MG, HMG, ECs, and HECs cultured in wells, as per literature [29, 30].

4.11. Measurement of TEER in TNF-α and ARVA Groups

The TEER of confluent cell barriers was measured once a day for the first 3 days. On the third day, a solution of TNF-α at 5ng/mL or ARVA at 1μg/mL diluted in media was added to the apical (top) and bottom side of the transwell of each cell barrier group, followed by TEER measurements at 1hr, 3 hr, 6 hr, and 24 hr. After recording the 24hr time point, the treatment solution from each transwell and was removed and transwells were placed in DPBS for 2 minutes. Fresh media was replaced with each group's respective media (basal or hyperglycemic) and TEER was recorded until Day 6 of the study. Barrier recovery was measured by the percent change of TEER from the last treatment time point (24 hr) to the measured TEER value on Day 6.

4.12. Imaging and Software

An epifluorescence microscope (Leica DMi8) with a cooled CCD camera (DFC7000 GT, Leica) and LAS X Science microscope software was used to capture images in both brightfield and fluorescence via 10X or 20X objective. Fluorescence intensity was quantified using DAPI, GFP, TXR, and CY5 filters matching the corresponding fluorophore for the immunocytochemistry

studies. Intensity values (16-bit: 0-65535) of fluorescence expression were measured using ImageJ (NIH) by measuring the corrected total cell fluorescence (CTCF) using equation (3):

$$\text{CTCF} = [I_D - (A_C * \bar{F}_B] \quad (3)$$

Where ID is the integrated fluorescence density (arbitrary units) of a cell, Ac is the surface area (μm^2) of a cell, and FB is the mean fluorescence background readings (arbitrary units) surrounding the cell, as measured in previous studies [41, 42].

4.13. Statistical Analysis and Software

Two-way ANOVA was used to analyze statistical significance among groups at different time-points (e.g., TEER assays). Two-way ANOVA repeated measures was used to determine the effect of the hyperglycemic medium on cell area over time on the treated groups (e.g., cell area change of HMG from Day 1 to Day 6). One-way ANOVA was also used to assess parametric data from single-time point studies (e.g. immunocytochemistry). Post-hoc Tukey test was performed to identify the level of statistical significance among the groups. Each study included a minimum of 45 cells with at least 3 replicates per experimental condition for the cell morphology studies. Immunocytochemistry assays used at least 10 cells from 5 different regions (grid) of the well with 3 replicates per condition. Cell barrier assays included at least 3 replicates per condition with 3 readings per replicate from different regions of the transwell. Statistical significance is denoted by symbols: * or †, where $p < 0.05$ = * or †, $p < 0.01$ = ** or ††, $p < 0.001$ = ***, $p < 0.0001$ = ****, n.s. = not statistically significant. All statistical tests were performed using GraphPad Prism 10 software.

5. Conclusion

The effects of AGEs from chronic hyperglycemia are well-known to cause cell apoptosis and dysfunction that are compounded in barrier tissue. This study illustrates significant cell and molecular relationships between cell barriers of Müller glia and endothelial cells critical to the response and function of the inner blood retinal barrier in hyperglycemia. Our data illustrate unexplored impacts of Müller glia communication with endothelial cells in barrier resistivity and highlight the significance of this glial vascular unit to development of combinatory therapies for diabetic retinopathy.

Supplementary Materials: The following supporting information can be downloaded at: www.mdpi.com/xxx/s1, Supplemental Figure S-1. Summary of (A) cell area changes and (B) cell shape index over time for endothelial cells (ECs) and Müller glia (MG) under control (or normoglycemic) and hyperglycemic (H) conditions.

Author Contributions: Conceptualization, J.S.P. and M.V.; methodology, J.S.P., M.V., and F.B.; Software, J.S.P..; validation, J.S.P., M.V., and F.B.; formal analysis, J.S.P. and M.V.; investigation, J.S.P.; resources, M.V. and F.B..; data curation, J.S.P.; writing—original draft preparation, J.S.P.; writing—review and editing, M.V. and F.B..; visualization, J.S.P., M.V., and F.B.; supervision, M.V. and F.B.; project administration, M.V.; funding acquisition, M.V. and F.B. All authors have read and agreed to the published version of the manuscript.

Funding: This research and APC were funded by the U.S. National Science Foundation, CBET 2243644, and the New Jersey Health Foundation, PC 140-24.

Data Availability Statement: The original contributions presented in the study are included in the article/supplementary material, further inquiries can be directed to the corresponding author.

Conflicts of Interest: The authors declare no conflicts of interest.

References

1. Teo, Z.L., Y.C. Tham, M. Yu, M.L. Chee, T.H. Rim, N. Cheung, M.M. Bikbov, Y.X. Wang, Y. Tang, Y. Lu, I.Y. Wong, D.S.W. Ting, G.S.W. Tan, J.B. Jonas, C. Sabanayagam, T.Y. Wong, and C.Y. Cheng, *Global Prevalence of Diabetic Retinopathy and Projection of Burden through 2045: Systematic Review and Meta-analysis*. Ophthalmology, 2021. **128**(11): p. 1580-1591.
2. Wei, L., X. Sun, C. Fan, R. Li, S. Zhou, and H. Yu, *The pathophysiological mechanisms underlying diabetic retinopathy*. Front Cell Dev Biol, 2022. **10**: p. 963615.
3. Diaz-Coranguez, M., C. Ramos, and D.A. Antonetti, *The inner blood-retinal barrier: Cellular basis and development*. Vision Res, 2017. **139**: p. 123-137.
4. Garcia-Bermudez, M.Y., K.K. Freude, Z.A. Mouhammad, P. van Wijngaarden, K.K. Martin, and M. Kolko, *Glial Cells in Glaucoma: Friends, Foes, and Potential Therapeutic Targets*. Front Neurol, 2021. **12**: p. 624983.
5. Roy, S., D. Kim, and R. Lim, *Cell-cell communication in diabetic retinopathy*. Vision Res, 2017. **139**: p. 115-122.
6. Mengstie, M.A., E. Chekol Abebe, A. Behaile Teklemariam, A. Tilahun Mulu, M.M. Agidew, M. Teshome Azezew, E.A. Zewde, and A. Agegnehu Teshome, *Endogenous advanced glycation end products in the pathogenesis of chronic diabetic complications*. Front Mol Biosci, 2022. **9**: p. 1002710.
7. Shahriyary, L., G. Riazi, M.R. Lornejad, M. Ghezlou, B. Bigdeli, B. Delavari, F. Mamashli, S. Abbasi, J. Davoodi, and A.A. Saboury, *Effect of glycated insulin on the blood-brain barrier permeability: An in vitro study*. Arch Biochem Biophys, 2018. **647**: p. 54-66.
8. Agarwal, D., R. Gelman, C. Prospero Ponce, W. Stevenson, and J.B. Christoforidis, *The Vitreomacular Interface in Diabetic Retinopathy*. J Ophthalmol, 2015. **2015**: p. 392983.
9. Jiang, Y., L. Liu, and J.J. Steinle, *Compound 49b Regulates ZO-1 and Occludin Levels in Human Retinal Endothelial Cells and in Mouse Retinal Vasculature*. Invest Ophthalmol Vis Sci, 2017. **58**(1): p. 185-189.
10. Vinken, M., E. Decrock, L. Leybaert, G. Bultynck, B. Himpens, T. Vanhaecke, and V. Rogiers, *Non-channel functions of connexins in cell growth and cell death*. Biochim Biophys Acta, 2012. **1818**(8): p. 2002-8.
11. Albert-Garay, J.S., J.R. Riesgo-Escovar, and R. Salceda, *High glucose concentrations induce oxidative stress by inhibiting Nrf2 expression in rat Muller retinal cells in vitro*. Sci Rep, 2022. **12**(1): p. 1261.
12. Portillo, J.A., J.A. Greene, G. Okenka, Y. Miao, N. Sheibani, T.S. Kern, and C.S. Subauste, *CD40 promotes the development of early diabetic retinopathy in mice*. Diabetologia, 2014. **57**(10): p. 2222-31.

13. Zong, H., M. Ward, A. Madden, P.H. Yong, G.A. Limb, T.M. Curtis, and A.W. Stitt, *Hyperglycaemia-induced pro-inflammatory responses by retinal Muller glia are regulated by the receptor for advanced glycation end-products (RAGE)*. Diabetologia, 2010. **53**(12): p. 2656-66.
14. Dobi, A., S. Rosanaly, A. Devin, P. Baret, O. Meilhac, G.J. Harry, C.L. d'Hellencourt, and P. Rondeau, *Advanced glycation end-products disrupt brain microvascular endothelial cell barrier: The role of mitochondria and oxidative stress.* Microvasc Res, 2021. **133**: p. 104098.
15. Sang, H.Q., J.F. Gu, J.R. Yuan, M.H. Zhang, X.B. Jia, and L. Feng, *The protective effect of Smilax glabra extract on advanced glycation end products-induced endothelial dysfunction in HUVECs via RAGE-ERK1/2-NF-kappaB pathway.* J Ethnopharmacol, 2014. **155**(1): p. 785-95.
16. Yamazaki, Y., H. Wake, T. Nishinaka, O.F. Hatipoglu, K. Liu, M. Watanabe, T. Toyomura, S. Mori, T. Yoshino, M. Nishibori, and H. Takahashi, *Involvement of multiple scavenger receptors in advanced glycation end product-induced vessel tube formation in endothelial cells*. Exp Cell Res, 2021. **408**(1): p. 112857.
17. Pena, J.S., R.K. Ramanujam, R.A. Risman, V. Tutwiler, F. Berthiaume, and M. Vazquez, *Neurovascular Relationships in AGEs-Based Models of Proliferative Diabetic Retinopathy.* Bioengineering (Basel), 2024. **11**(1).
18. Dierschke, S.K., A.L. Toro, W.P. Miller, S. Sunilkumar, and M.D. Dennis, *Diabetes enhances translation of Cd40 mRNA in murine retinal Muller glia via a 4E-BP1/2-dependent mechanism*. J Biol Chem, 2020. **295**(31): p. 10831-10841.
19. Komarova, Y.A., K. Kruse, D. Mehta, and A.B. Malik, *Protein Interactions at Endothelial Junctions and Signaling Mechanisms Regulating Endothelial Permeability.* Circ Res, 2017. **120**(1): p. 179-206.
20. Rudraraju, M., S.P. Narayanan, and P.R. Somanath, *Regulation of blood-retinal barrier cell-junctions in diabetic retinopathy.* Pharmacol Res, 2020. **161**: p. 105115.
21. Shen, H., Q. Gong, J. Zhang, H. Wang, Q. Qiu, J. Zhang, and D. Luo, *TRIM46 aggravated high glucose-induced hyper permeability and inflammatory response in human retinal capillary endothelial cells by promoting IkappaBalpha ubiquitination*. Eye Vis (Lond), 2022. **9**(1): p. 35.
22. Rom, S., N.A. Heldt, S. Gajghate, A. Seliga, N.L. Reichenbach, and Y. Persidsky, *Hyperglycemia and advanced glycation end products disrupt BBB and promote occludin and claudin-5 protein secretion on extracellular microvesicles.* Sci Rep, 2020. **10**(1): p. 7274.
23. Strauss, R.E. and R.G. Gourdie, *Cx43 and the Actin Cytoskeleton: Novel Roles and Implications for Cell-Cell Junction-Based Barrier Function Regulation*. Biomolecules, 2020. **10**(12).
24. Epifantseva, I. and R.M. Shaw, *Intracellular trafficking pathways of Cx43 gap junction channels*. Biochim Biophys Acta Biomembr, 2018. **1860**(1): p. 40-47.
25. Tretiach, M., M.C. Madigan, and M.C. Gillies, *Conditioned medium from mixed retinal pigmented epithelium and Muller cell cultures reduces in vitro permeability of retinal vascular endothelial cells.* Br J Ophthalmol, 2004. **88**(7): p. 957-61.
26. Fresta, C.G., A. Fidilio, G. Caruso, F. Caraci, F.J. Giblin, G.M. Leggio, S. Salomone, F. Drago, and C. Bucolo, *A New Human Blood-Retinal Barrier Model Based on Endothelial Cells, Pericytes, and Astrocytes.* Int J Mol Sci, 2020. **21**(5).
27. Coughlin, B.A., D.J. Feenstra, and S. Mohr, *Muller cells and diabetic retinopathy.* Vision Res, 2017. **139**: p. 93-100.
28. Garvin, J., M. Semenikhina, Q. Liu, K. Rarick, E. Isaeva, V. Levchenko, A. Staruschenko, O. Palygin, D. Harder, and S. Cohen, *Astrocytic responses to high glucose impair barrier formation in cerebral microvessel endothelial cells.* Am J Physiol Regul Integr Comp Physiol, 2022. **322**(6): p. R571-R580.

29. Guo, B., Y. Wang, Y. Hui, X. Yang, and Q. Fan, *Effects of anti-VEGF agents on rat retinal Muller glial cells.* Mol Vis, 2010. **16**: p. 793-9.
30. Iriyama, A., Y.N. Chen, Y. Tamaki, and Y. Yanagi, *Effect of anti-VEGF antibody on retinal ganglion cells in rats.* Br J Ophthalmol, 2007. **91**(9): p. 1230-3.
31. Liu, S., Y. Ju, and P. Gu, *Experiment-Based Interventions to Diabetic Retinopathy: Present and Advances.* Int J Mol Sci, 2022. **23**(13).
32. Pereiro, X., N. Ruzafa, A. Acera, A. Urcola, and E. Vecino, *Optimization of a Method to Isolate and Culture Adult Porcine, Rats and Mice Muller Glia in Order to Study Retinal Diseases.* Front Cell Neurosci, 2020. **14**: p. 7.
33. Chiang, M.Y., Y. Yangben, N.J. Lin, J.L. Zhong, and L. Yang, *Relationships among cell morphology, intrinsic cell stiffness and cell-substrate interactions.* Biomaterials, 2013. **34**(38): p. 9754-62.
34. Pena, J.S., D. Robles, S. Zhang, and M. Vazquez, *A Milled Microdevice to Advance Glia-Mediated Therapies in the Adult Nervous System.* Micromachines (Basel), 2019. **10**(8).
35. Lorenz, L., S. Hirmer, A. Schmalen, S.M. Hauck, and C.A. Deeg, *Cell Surface Profiling of Retinal Muller Glial Cells Reveals Association to Immune Pathways after LPS Stimulation.* Cells, 2021. **10**(3).
36. Dauphinee, S.M. and A. Karsan, *Lipopolysaccharide signaling in endothelial cells.* Lab Invest, 2006. **86**(1): p. 9-22.
37. Colas-Algora, N., D. Garcia-Weber, C. Cacho-Navas, S. Barroso, A. Caballero, C. Ribas, I. Correas, and J. Millan, *Compensatory increase of VE-cadherin expression through ETS1 regulates endothelial barrier function in response to TNFalpha.* Cell Mol Life Sci, 2020. **77**(11): p. 2125-2140.
38. Ge, S., X. Jiang, D. Paul, L. Song, X. Wang, and J.S. Pachter, *Human ES-derived MSCs correct TNF-alpha-mediated alterations in a blood-brain barrier model.* Fluids Barriers CNS, 2019. **16**(1): p. 18.
39. Xu, S.Q., K. Mahadev, X. Wu, L. Fuchsel, S. Donnelly, R.G. Scalia, and B.J. Goldstein, *Adiponectin protects against angiotensin II or tumor necrosis factor alpha-induced endothelial cell monolayer hyperpermeability: role of cAMP/PKA signaling.* Arterioscler Thromb Vasc Biol, 2008. **28**(5): p. 899-905.
40. Stefanini, F.R., J.F. Arevalo, and M. Maia, *Bevacizumab for the management of diabetic macular edema.* World J Diabetes, 2013. **4**(2): p. 19-26.
41. Jakic, B., M. Buszko, G. Cappellano, and G. Wick, *Elevated sodium leads to the increased expression of HSP60 and induces apoptosis in HUVECs.* PLoS One, 2017. **12**(6): p. e0179383.
42. McCloy, R.A., S. Rogers, C.E. Caldon, T. Lorca, A. Castro, and A. Burgess, *Partial inhibition of Cdk1 in G 2 phase overrides the SAC and decouples mitotic events.* Cell Cycle, 2014. **13**(9): p. 1400-12.

Figure 1. Structure of the inner Blood Retinal Barrier (iBRB) and communication between endothelial cells (ECs) and Müller glia (MG) in basal and hyperglycemic conditions. A) Schematic of the retina and iBRB anatomy. The inner blood retinal barrier is mainly comprised of endothelial cells, pericytes, a basement membrane, and the foot processes of glial cells. The iBRB is a uniform capillary bed extending from the nerve fiber layer to the inner nuclear layer. The foot processes of astrocytes reside on the nerve fiber layer, while the foot processes of Muller glia are throughout the iBRB.

B) MG and EC communication at the iBRB. MG communicate with each other and with endothelial cells via gap junctions formed by connexin 43 (CX-43), while ECs communicate largely via zonula occludens-1 (ZO-1). In hyperglycemic conditions, the expression of gap junctions in MG is disrupted by abnormal junction formation of CX-43. Likewise, the expression of ZO-1 is decreased in hyperglycemic ECs, resulting in higher permeability across the capillary wall.

Figure 2. Morphology Changes in Müller Glia (MG) and Endothelial Cells (ECs) in Response to Hyperglycemic Conditions formed using High Glucose and Advanced Glycation End-Products (AGEs). A) Reactive Oxygen Species (ROS) expression in MG and ECs in response to different concentrations of hyperglycemic media: 25mM glucose and either 1μg/mL, 5 μg/mL, or 10 μg/mL of advanced glycation end-products (AGEs) after 6 days of culture. Ultimately the condition of 25mM glucose + 1μg/mL AGEs was chosen as the hyperglycemic media for this study. **B)** Representative brightfield and fluorescence images of ROS expression in **B1)** Müller glia (MG), **B2)** hyperglycemic MG (HMG) – MG exposed to hyperglycemic media, **B3)** endothelial cells (ECs), and **B4)** hyperglycemic ECs (HECs) – ECs exposed to hyperglycemic media, after 6 days in culture with hyperglycemic media. **C1)** Changes in surface area of MG, ECs, HMG, and HECs in response to control media (5mM glucose) and hyperglycemic media (25mM glucose+1μg/mL AGEs). **C2)** Changes in cell morphology over time measured by cell shape index (CSI) of MG, HMG, ECs, and HECs in response to control media (5mM glucose) and hyperglycemic media

(25mM glucose+1μg/mL AGEs. **D)** Brightfield images of **D1)** MG, **D2)** HMG, **D3)** ECs, and **D4)** HECs 24 hr post-seeding in culture wells. Scale bar is 100μm. *p< 0.05, **p< 0.01.

Figure 3. RAGE and CD-40 Expression in ECs, HECs, MG, and HMG. RAGE expression in **A)** endothelial cells (ECs), hyperglycemic endothelial cells (HECs), **B)** Muller glia (MG), and hyperglycemic-induced Muller glia (HMG) cultured in hyperglycemic media (25mM glucose and 1μg/mL AGEs) for 15 days. **C)** Normalized fluorescence intensity per cell area (%) correlating RAGE expression in all cell groups. CD-40 expression in **D)** ECs, HECs, **E)** MG, and HMG cultured in hyperglycemic media (25mM glucose and 1μg/mL AGEs) for 15 days. **F)** Normalized fluorescence intensity per cell area (%) correlating CD-40 expression in all cell groups. IgG was utilized as a negative immunostaining control. Scale bar is 100μm. *p< 0.05, **p< 0.01.

Figure 4. Expression of Zonula Occludens 1 (ZO-1) and Connexin-43 (CX43) Expression in Müller glia (MG) and Endothelial Cells (ECs). A1) ZO-1 expression in ECs in response to hyperglycemic condition (25mM glucose+1μg/mL AGEs), and staining controls (Isotype control and No primary antibody). Yellow arrowheads point towards disruption of ZO-1 boundaries between adjacent cells. White arrowheads point to clustering of ZO-1. **A2)** Quantification of ZO-1 in ECs via integrated fluorescence intensity/area. **B1)** CX43 expression in ECs in response to hyperglycemic condition (25mM glucose+1μg/mL AGEs), and controls (Isotype control and No primary antibody). **B2)** Quantification of CX43 in ECs via integrated fluorescence intensity/area. **C1)** CX43 expression in MG in response to hyperglycemic condition (25mM glucose+1μg/mL AGEs), and controls (Isotype control and no primary antibody). **C2)** Quantification of CX43 in MG via integrated fluorescence intensity/area. Scale bar is 100μm. * p< 0.05, ** p< 0.01, *** p< 0.001, **** p< 0.0001.

Figure 5. Measurement of Barrier Integrity via Trans-Endothelial/Epithelial Resistance (TEER). A) Schematic depicting the transwell configurations of cell barriers, ECM: transwell membrane coated with

fibronectin and collagen IV at a 1:1 ratio, 1mg/mL, ECs: Endothelial cells monolayers on coated membranes with ECM. MG: Müller glia monolayers on coated membranes with ECM. COMBO: ECs monolayer on top of an ECM coated membrane + MG monolayer on the bottom of the same membrane. **B)** TEER quantification of **B1)** normoglycemic and **B2)** hyperglycemic groups, **B3)** overlap of normoglycemic and hyperglycemic cell barriers over the course of 7 days. Statistically significant differences between COMBO and ECs are compared in B1, and between hyperglycemic COMBO and HECs are compared in B2. Statistical differences between normoglycemic and hyperglycemic groups of the same cell type (e.g., MG and HMG) are compared in B3. * ($p<0.05$), ** ($p<0.01$), *** ($p<0.001$), and **** ($p<0.0001$).

Figure 6. Barrier Recovery Response to TNF-α and ARVA via Trans-Endothelial/Epithelial Resistance (TEER). A) TEER quantification of cell barriers in the presence of TNF-α (5ng/mL) in **A1)** normoglycemic groups (solid lines) and **A2)** hyperglycemic groups (dashed lines). ECM: transwell membrane coated with fibronectin and collagen IV at a 1:1 ratio, 1mg/mL, ECs: Endothelial cells monolayers on coated membranes with ECM. MG: Müller glia monolayers on coated membranes with ECM. COMBO: ECs monolayer on top of an ECM coated membrane + MG monolayer on the bottom of the same membrane. **B)** TEER quantification of cell barriers in the presence of Anti-Rat Vegf-A (ARVA) (1µg/mL) in normoglycemic groups (solid lines) and hyperglycemic groups (dashed lines). COMBO: ECs monolayer on top of an ECM coated membrane + MG monolayer on the bottom of the same membrane. Hyperglycemic COMBO: COMBO in hyperglycemic conditions. COMBO + ARVA: COMBO treated with ARVA (1µg/mL). Hyperglycemic COMBO + ARVA: hyperglycemic COMBO treated with ARVA (1µg/mL). ΔΩ is the percent TEER recovery, measured by the TEER change between day 4 and day 6. ΔΩ = COMBO, ΔΩ C+A = COMBO +ARVA, ΔΩ D = Hyperglycemic COMBO, and ΔΩ DC + A = Hyperglycemic COMBO +ARVA. **** ($p< 0.0001$) correspond to the statistical difference between hyperglycemic COMBO and hyperglycemic COMBO + ARVA.

Supplemental Figure S-1. Summary of (A) cell area changes and (B) cell shape index over time for endothelial cells (ECs) and Müller glia (MG) under control (or normoglycemic) and hyperglycemic (H) conditions.

A Day	ECs: Control (μm^2)	HECs (μm^2)	MG: Control (μm^2)	HMG (μm^2)	p-values (ECs)	p-values (MG)
0	291.03 ± 104.01	1,552.61 ± 444.51	339.09 ± 176.32	1,431.82 ± 1,556.07	ns	ns
1	1,726.07 ± 441.22	1,438.61 ± 240.18	3,548.58 ± 1,620.65	3,384.83 ± 1,874.50	ns	ns
2	2,062.59 ± 756.26	1,523.53 ± 347.49	4,589.17 ± 1,847.62	3,424.59 ± 1,638.37	ns	ns
4	1,712.33 ± 462.09	540.77 ± 222.87	2,709.51 ± 861.25	5,741.33 ± 2,158.06	ns	****
6	1,459.61 ± 386.96	482.60 ± 120.73	4,837.92 ± 3,333.75	10,937.68 ± 2,613.82	ns	****

B Day	ECs: Control	HECs	MG: Control	HMG	p-values (ECs)	p-values (MG)
0	0.95 ± 0.03	0.62 ± 0.25	0.49 ± 0.08	0.54 ± 0.28	***	ns
1	0.50 ± 0.17	0.41 ± 0.20	0.30 ± 0.17	0.36 ± 0.21	ns	ns
2	0.32 ± 0.15	0.52 ± 0.26	0.30 ± 0.28	0.25 ± 0.14	ns	ns
4	0.30 ± 0.14	0.73 ± 0.12	0.24 ± 0.12	0.29 ± 0.12	****	ns
6	0.28 ± 0.13	0.77 ± 0.08	0.31 ± 0.13	0.39 ± 0.09	****	ns